AIAA JOURNAL
Vol. 45, No. 6, June 2007

Three-Dimensional Turbulent Wall Jets Issuing from Moderate-Aspect-Ratio Rectangular Channels

Joseph W. Hall* and Daniel Ewing†
McMaster University, Hamilton, Ontario L8S 4L7, Canada

DOI: 10.2514/1.20386

The development of three-dimensional turbulent wall jets emanating from long channels with outlet cross-sectional aspect ratios from 1 to 8 was investigated by measuring the mean and turbulent flowfields using hot-wire anemometry. The turbulent velocity profiles indicate that the core of the jet behaves like a two-dimensional wall jet before the interaction of the lateral shear layers. Contours of the full flowfield indicate that the turbulent mechanism that causes the lateral growth of the three-dimensional wall jets is located in the lateral shear layers near the wall. Increasing the outlet aspect ratio separates the lateral shear layers, causing a wider core region of two-dimensional wall-jet development that, in turn, delays the onset of far-field three-dimensional wall-jet development. The development of the different aspect-ratio wall jets collapsed onto a single curve when the streamwise coordinate was normalized by the square root of the channel cross-sectional area and the vertical and lateral jet half-widths were normalized by the height and width of the channel, respectively.

Nomenclature

A	=	channel cross-sectional area, m^2
A_R	=	channel aspect ratio, W/h
h	=	height of channel, m
Re_h	=	Reynolds number, $U_{\text{exit}}h/\nu$
U_{exit}	=	exit streamwise velocity, m/s
U_{max}	=	local maximum streamwise velocity, m/s
U_o	=	bulk velocity of the jet, m/s
u_{rms}	=	standard deviation of turbulent streamwise velocity, m/s
W	=	width of channel, m
x	=	streamwise coordinate, m
y	=	vertical coordinate, m
y_{max}	=	height of U_{max}, m
$y_{1/2}$	=	vertical jet half-width, m
z	=	lateral coordinate, m
$z_{1/2}$	=	lateral jet half-width, m
ν	=	kinematic viscosity, m^2/s

I. Introduction

THREE-DIMENSIONAL wall jets are formed when a jet issues from a finite width nozzle and flows over a wall, as shown in Fig. 1. Three-dimensional wall jets occur in numerous practical applications such as high-lift systems, but are likely outweighed in economic importance by their use in heating, cooling, and ventilation applications. One of the most noteworthy features of turbulent three-dimensional wall jets is that the far-field lateral growth of the jet is typically five times greater than the growth normal to the wall [1,2]. The cause of this behavior is not fully understood but appears to be induced by strong turbulence-generated secondary motions in the jet [1–4]. The large lateral growth has been observed in three-dimensional wall jets emanating from round [5–8], square [9], triangular [9], and rectangular [10,11] outlets and thus does not appear to be sensitive to the outlet shape. The initial development of the three-dimensional wall jet, however, does depend on the jet-outlet geometry, and accurately predicting the jet development before the far field is important, for example, in thermal design applications. One approach is to use a virtual origin and then to normalize the streamwise coordinate by the square root of the outlet cross-sectional area, $\sqrt{A}$, a length scale related to the initial momentum flux of the jet [12]. This has proven reasonably successful at collapsing onto a single curve the observed streamwise variation of the jet half-widths and velocity decay of wall jets formed by differently shaped outlets with aspect ratios close to one [9] and for somewhat larger-aspect-ratio jets that were segments of a round, sharp-edged orifice [13,14]. A disadvantage of this technique is that it typically does not accurately predict the development of the jet as it grows from the outlet to the far field.

Few investigations compared the development of three-dimensional wall jets issuing from outlets with aspect ratios larger than one, despite the frequent occurrence of this flow in practice. In one such study, Padmanabham and Gowda [13,14] showed that the development of three-dimensional wall jets emanating from various segments of a round, sharp-edged orifice (and thus different aspect ratios) could be reasonably well described using the proposed $\sqrt{A}$ scaling and with a virtual origin correction. In two early studies, Viets and Sforza [10] and Sforza and Herbst [11] examined the development of three-dimensional wall jets exiting rectangular, sharp-edged orifices with aspect ratios of 10, 20, and 40, but did not compare them using $\sqrt{A}$ scaling. Based upon measurements of the centerline velocity decay, they proposed that there were three distinct streamwise regions of jet development, similar to the development of large-aspect-ratio free jets [15,16]. The first region was delineated by an approximately constant maximum mean streamwise velocity and associated with the jet potential core. This was followed by the characteristic decay region in which U_{max} began to decay, but not as quickly as in the radial decay (or far-field) region. Several authors have speculated that the development of the central portion of the wall jet in the characteristic decay region behaves like a two-dimensional wall jet because the lateral shear layers do not directly interact [11,12], but this has never been directly shown.

In the investigations of wall jets mentioned in the previous paragraph, all jets were formed using sharp-edged orifices [10,11,13,14]. It appears, though, that the development of these flows is not typical of wall jets formed by other exit conditions. For example, Launder and Rodi [1,2] found that the development of wall jets formed using sharp-edged orifices significantly differed from wall jets formed using long pipes or contoured nozzles. This finding

Received 5 October 2005; revision received 20 February 2007; accepted for publication 21 February 2007.

*Currently Department of Mechanical Engineering, University of New Brunswick, 15 Dineen Drive, Fredericton, NB, E3B 5A3, Canada; jwhall@unb.ca. Member AIAA.

†Currently Department of Mechanical and Materials Engineering, Queens University, Kingston, Ontario, Canada; ewingd@me.queensu.ca.

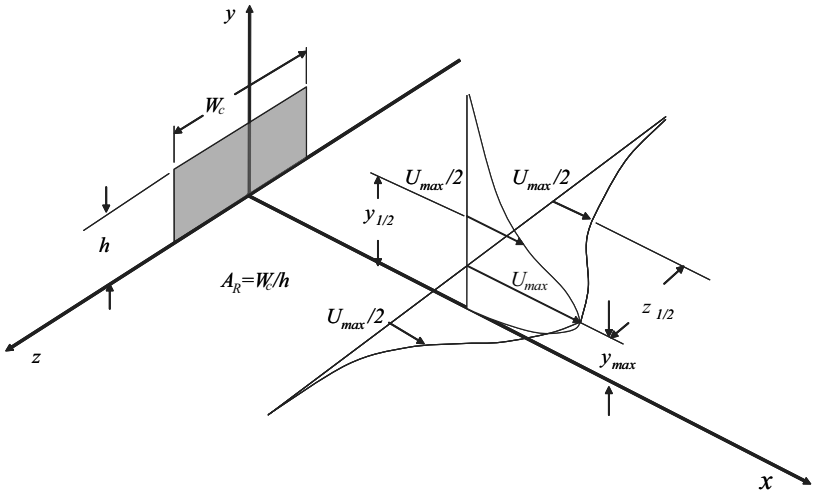

Fig. 1 Schematic of a three-dimensional wall jet issuing from a rectangular opening.

was later substantiated by Schwab [17], who found that the near field of an $A_R = 10$ wall jet was dominated by strong vortex structures that were specific to orifice jets. It was also found that the development of free jets and wall jets exiting sharp-edged orifices were sensitive to conditions upstream of the orifice and thus could be facility specific.

The objective of the present investigation was to examine how varying the outlet aspect ratio affects the initial development of three-dimensional wall jets. The measurements were performed using three-dimensional wall jets exiting from long channels to ensure that the boundary conditions at the jet outlet were well defined and consistent. Aspect ratios of 1, 3, 4, and 8 were used herein; the flow from the latter three aspect ratios were previously unexplored. The facility and methodology used in the investigation are described in the next section, followed by detailed measurements of the mean and turbulent velocities in the various jets. The conclusions of this investigation are then presented and discussed.

II. Experimental Setup

Airflow was supplied by a 7.5-kW variable-speed blower and conditioned using a 0.55 by 0.55 by 0.55 m settling chamber equipped with three foam filters, a 0.10-m-thick aluminum honeycomb flow straightener, and a fine wire mesh. Rather than using four different channels, a single channel with variable width was designed. The inside height of the channel was 2.54 cm and the internal width could be varied from 0 to 25.4 cm so that the aspect ratio could be continually varied from 0 to 10. The flow entered the channel through a specially designed bellmouth. The channel was 2.4-m-long ($96h$), and thus the flow exiting the channel was fully developed. Upon exiting the channel, the jet flowed over a horizontal

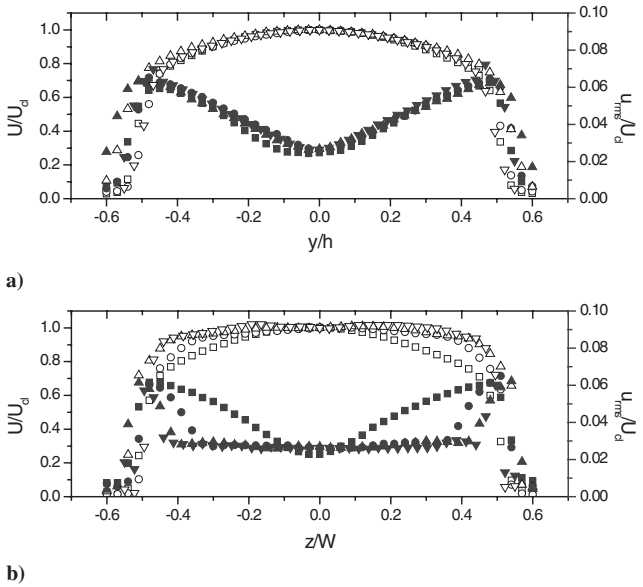

Fig. 2 Profiles of the mean (open symbols) and turbulent (filled symbols) streamwise velocities at $x/h = 0.1$ measured for the channel with $A_R = 1$ (□), $A_R = 3$ (○), $A_R = 4$ (△), and $A_R = 8$ (▽).

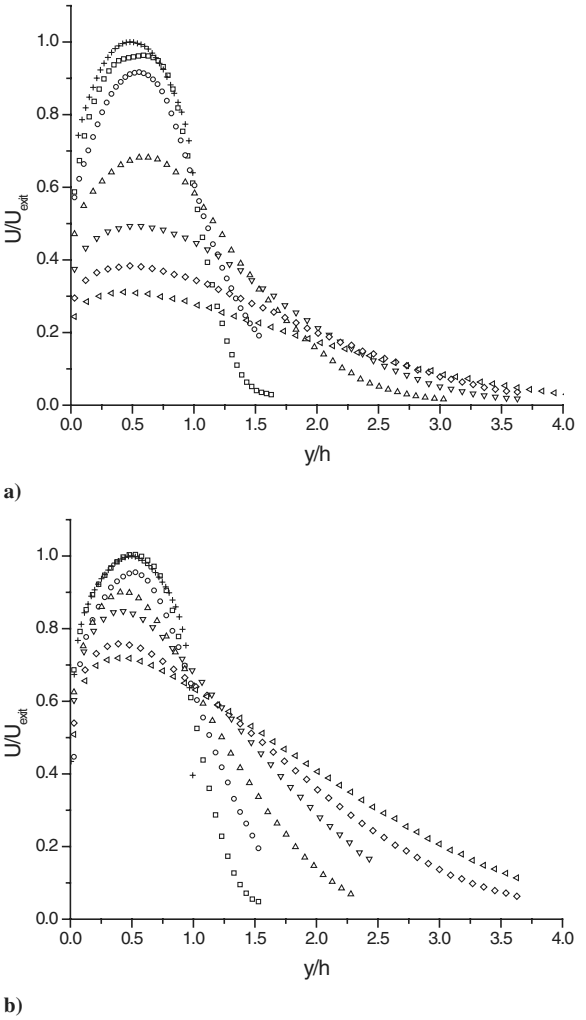

Fig. 3 Profiles of the mean streamwise velocity on the centerline of the jet at $x/h = 0.1$ (+), 3 (□), 6 (○), 10 (△), 15 (▽), 20 (◇), and 25 (◁) for the wall jets exiting the channel with a) $A_R = 1$ and b) $A_R = 8$.

plate with dimensions of 2.4 by 1.8 m. The bottom of the channel was mounted flush with the wall so that the jet interacted with the wall immediately after exiting the channel. A 1.2-m-high by 2.4-m-wide plate was mounted at the channel exit plane, preventing entrainment from behind the jet and yielding a well-defined jet-outlet condition.

The development of each wall jet was initially characterized by measuring streamwise velocity profiles along the jet centerline and laterally across the jet at the height of the maximum velocity, $y_{\max}$. An Auspex boundary-layer hot-wire probe was positioned using a computer-controlled traverse system with an accuracy of 0.05 mm. The in-house hot-wire anemometer was developed by Sun [18] using the design proposed by Perry [19]. The overheat ratio was set to 1.75 and the probe was calibrated in a separate facility. The temperature of the flow during the experiments was measured using a thermistor, and though the temperature variations during the measurements were less than ± 0.5°C, the effect of these changes on the velocity measurements was corrected using Beuther's [20] approach. The voltage output of the anemometer was filtered using an analog low-pass filter with a cutoff frequency of 5300 Hz and then sampled at 10,600 Hz using a 12-bit A/D board. The sampling time at the different downstream positions was adjusted so that the 95% confidence intervals for the estimates of the mean streamwise velocity at $y = y_{\max}$ were less than 0.2% on the centerline and less than 0.5% at the lateral half-width. The corresponding 95% confidence intervals for the estimates of the standard deviation of the velocity fluctuations, $u_{\rm rms}$, at these locations were less than 0.5 and 6%, respectively [21]. In the second phase of this investigation, the development of the wall jets was examined by measuring the streamwise velocity on a 41 by 21 grid that spanned the entire y–z plane of the jet. The sampling duration for these measurements was the same as for the velocity profiles, and thus, the uncertainties in the two sets of measurements were the same.

The measurements were performed with the aspect ratio of the channel set to $A_R = 1, 3, 4$, and 8. In all cases, the centerline velocity at the channel exit, $U_{\rm exit}$, was 55.0 m/s, corresponding to a Reynolds number based on the channel height and centerline velocity of $Re_h = 89,600$. Profiles of the mean and turbulent streamwise velocity measured on the vertical centerline and $y/h = 0.5$ at $x/h = 0.1$ for the different aspect-ratio channels are shown in Fig. 2. In all cases, the velocity profiles immediately downstream of the jet exit were symmetric and similar to those expected for fully developed channel flow. The bulk velocity for each jet was calculated by numerically integrating both mean profiles and then normalizing by the outlet cross-sectional area.

III. Experimental Results

The effect of varying the outlet aspect ratio on the development of the three-dimensional wall jets was first characterized using mean streamwise velocity profiles measured on the centerline of each jet. The profiles at $x/h = 0.1$ to 25 in the three-dimensional wall jets exiting the channels with $A_R = 1$ and $A_R = 8$ (referred to as the $A_R = 1$ and $A_R = 8$ wall jets, for brevity) are shown in Fig. 3. The rapid development of the $A_R = 1$ wall jet can be observed from the mean velocity profiles. For example, the profile at $x/h = 3$ in the $A_R = 8$ jet is almost identical to the profile at $x/h = 0.1$, whereas there is already a significant difference between the mean velocity

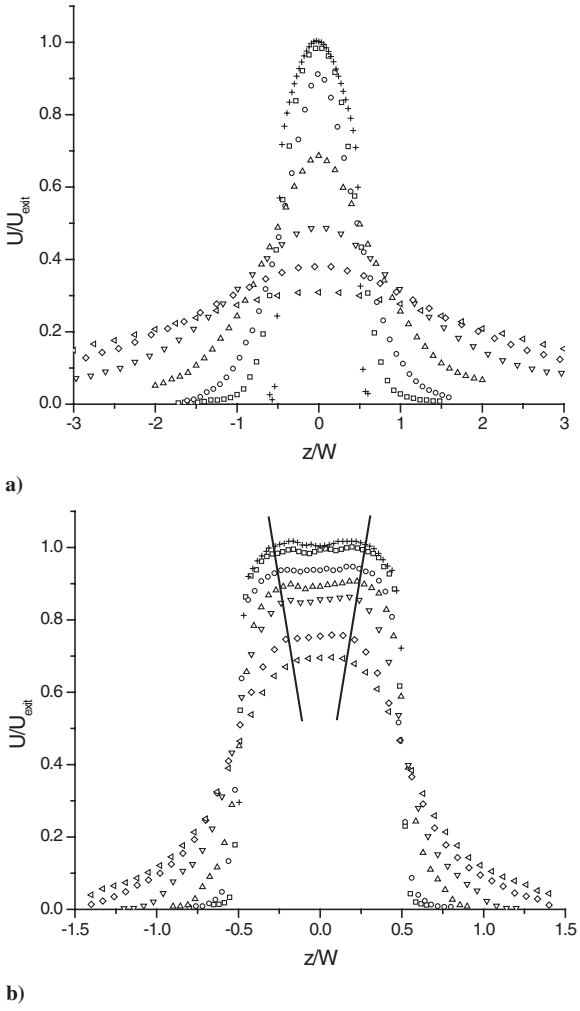

Fig. 4 Profiles of the mean streamwise velocity at $y = y_{\max}$ and $x/h = 0.1$ (+), 3 (□), 6 (○), 10 (△), 15 (▽), 20 (◇), and 25 (◁) for the wall jets exiting the channel with a) $A_R = 1$ and b) $A_R = 8$.

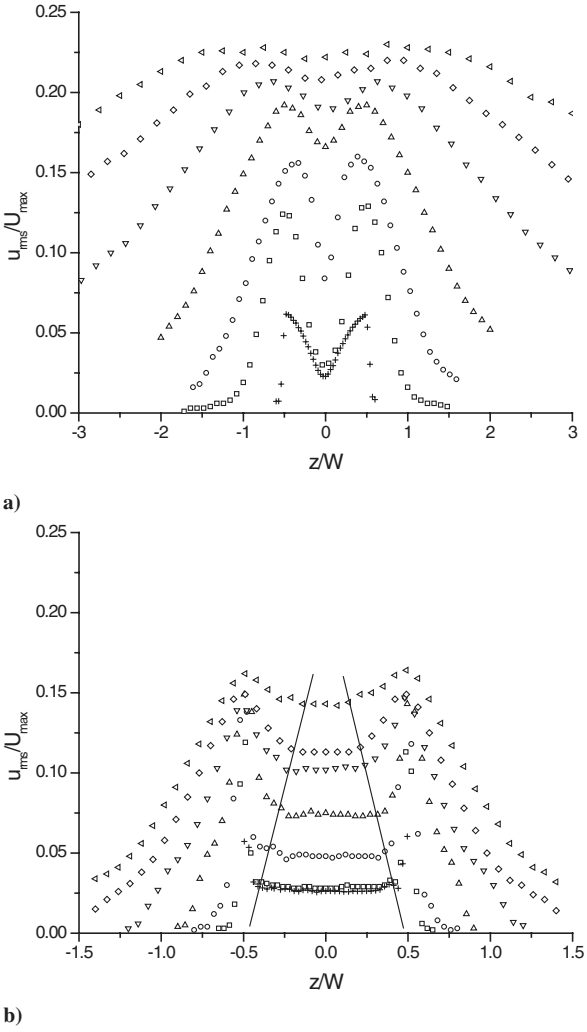

Fig. 5 Profiles of the turbulent streamwise velocity at $y = y_{\max}$ and $x/h = 0.1$ (+), 3 (□), 6 (○), 10 (△), 15 (▽), 20 (◇), and 25 (◁) for the wall jets exiting the channel with a) $A_R = 1$ and b) $A_R = 8$.

profiles in the $A_R = 1$ wall jet over the same range. The slower development of the larger-aspect-ratio wall jet is also evident from profiles of the mean velocity measured laterally across the jet at y_{max} (Fig. 4). The $A_R = 1$ jet spreads continually, whereas the larger-aspect-ratio jet develops only at the edges, causing a central region of reasonably uniform velocity, indicated by the bold lines. There were also differences in the behavior of the peak in the velocity profiles for the two wall jets. In particular, the value of y_{max} continually decreases for the $A_R = 8$ jet, whereas the value increases slightly before decreasing in the $A_R = 1$ jet.

The central region of development in the $A_R = 8$ wall jet can be better observed in the turbulent velocity profiles shown in Fig. 5. The turbulent fluctuations increase uniformly in the central region as the flow evolves downstream, whereas the fluctuations on the outer edges of the jet are more consistent with shear-layer development. The distance between the peaks in the profiles indicate that the shear layers on the lateral edges of this jet have not interacted even as far downstream as $x/h = 25$. The behavior is quite different in the $A_R = 1$ jet; the maxima in the turbulent velocity profiles associated with the lateral shear layers increase quite rapidly and begin to move away from the jet centerline at $x/h \approx 15$ and there is no discernible region of uniform turbulent velocity fluctuations at the center of the jet.

The turbulent velocity profiles on the centerline of both of these wall jets are shown in Fig. 6. In both jets, the fluctuations associated with the outer shear layers initially grew much faster than the peak near the wall. The magnitude of the fluctuations near the wall in the $A_R = 1$ wall jet grew rapidly between $x/h = 6$ and 10, becoming comparable to the fluctuations in the outer shear layer. Thereafter, the fluctuations in both the inner and outer layers increased. This differed significantly from the behavior of the profiles in the $A_R = 8$ wall jet, in which the fluctuations near the wall remained significantly smaller than those in the outer shear layer, even as far downstream as $x/h = 25$. As discussed later, this behavior is more consistent with two-dimensional wall-jet development than three-dimensional wall-jet development.

The development of the local maximum velocity and the growth of the jet half-widths in all jets investigated are compared in Fig. 7. The velocity was normalized by the bulk velocity at the jet exit, and the streamwise coordinate and length scales were normalized by a height of the channel, a common two-dimensional wall-jet scaling. The slower development of the larger-aspect-ratio jets is clear: at $x/h =$ 30 to 40, the $A_R = 1$ wall jet is wider than either the $A_R = 3$ or 4 wall jets. The normalized vertical half-widths in the larger-aspect-ratio jets collapsed onto a single line and in all cases grew in an approximately linearly fashion. The vertical half-widths for the $A_R = 1$ wall jet differed somewhat from the larger-aspect-ratio jets between $x/h = 10$ and 20, likely due to the rapid development of this flow.

The decay of the local maximum mean velocity with the streamwise coordinate normalized by the proposed $\sqrt{A}$ scaling is shown in Fig. 8. Despite the fact that some momentum must be lost to the wall, the observed values of the decay of the maximum velocity

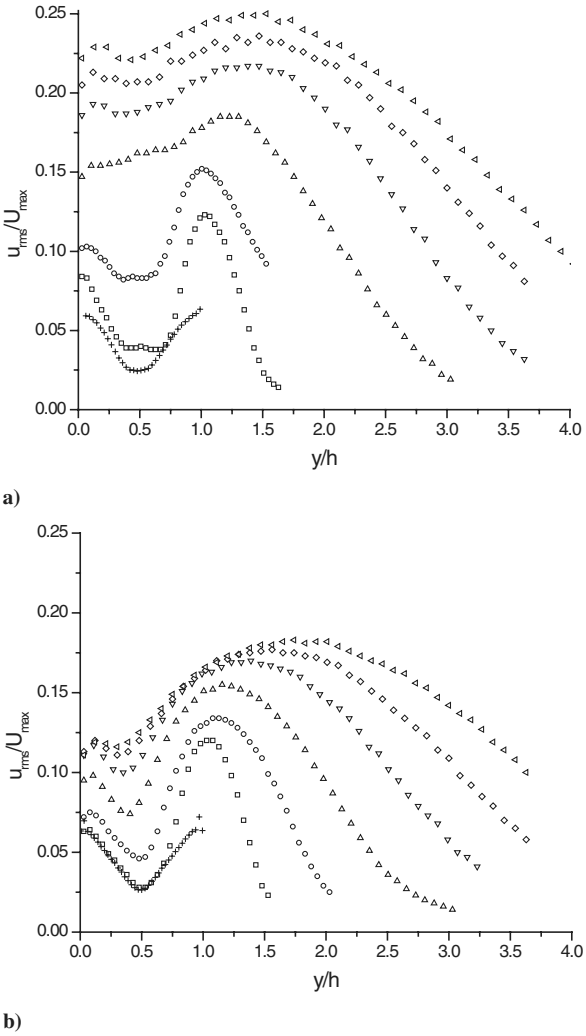

Fig. 6 Profiles of the turbulent streamwise velocity on the centerline at $x/h = 0.1$ (+), 3 (□), 6 (○), 10 (△), 15 (▽), 20 (◇), and 25 (◁) for the wall jets exiting the channel with a) $A_R = 1$ and b) $A_R = 8$.

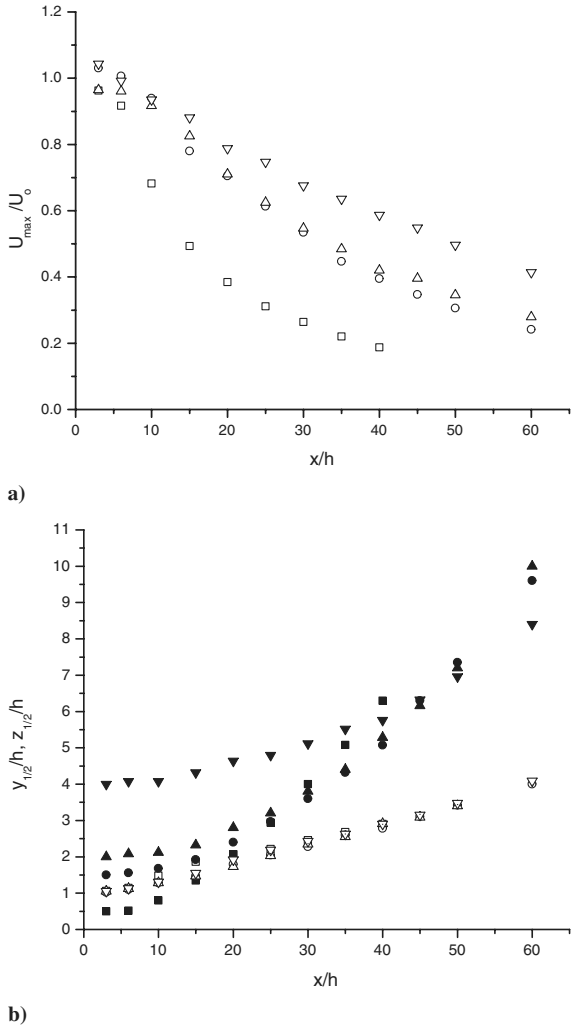

Fig. 7 Streamwise development of the a) maximum velocity point and b) vertical half-widths (open symbols) and lateral half-widths (filled symbols) for the wall jets exiting the channel with $A_R = 1$ (□), $A_R = 3$ (○), $A_R = 4$ (△), and $A_R = 8$ (▽).

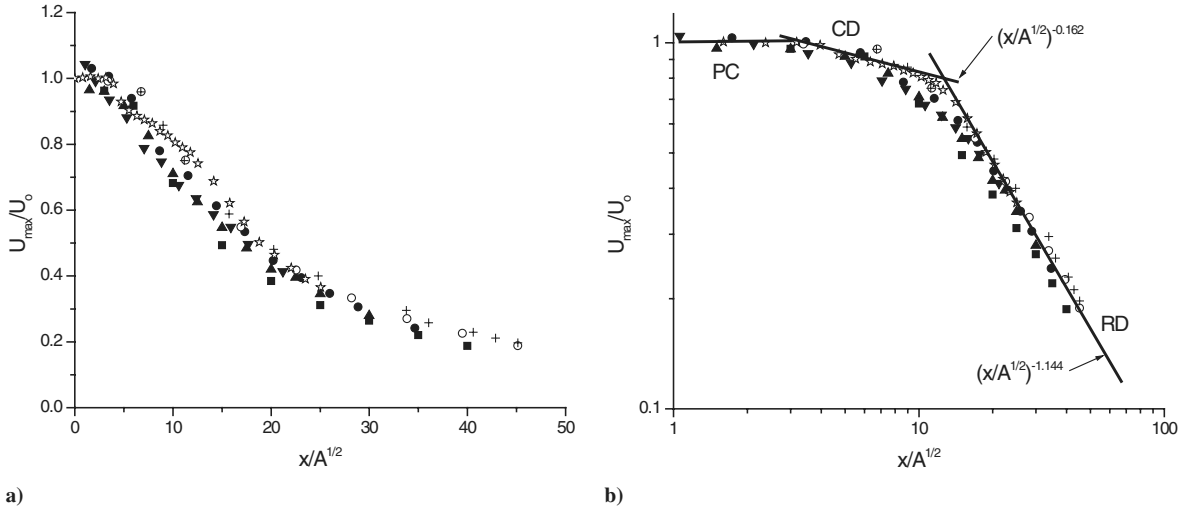

Fig. 8 Normalized streamwise development of the maximum velocity point in wall jets exiting the channel with $A_R = 1$ (■), $A_R = 3$ (●), $A_R = 4$ (▲), and $A_R = 8$ (▼), compared with previous results for wall jets exiting an $A_R = 1$ channel and $Re_h = 6 \times 10^4$ [22] (□), sharp-edged orifice with $A_R = 10$ and $Re_h = 3.4 \times 10^4$ [10] (★), wall jet exiting a round pipe with $Re_D = 1.1 \times 10^5$ [7] (○), and a wall jet exiting a round contoured nozzle with $Re_D = 1.7 \times 10^5$ [6] (+).

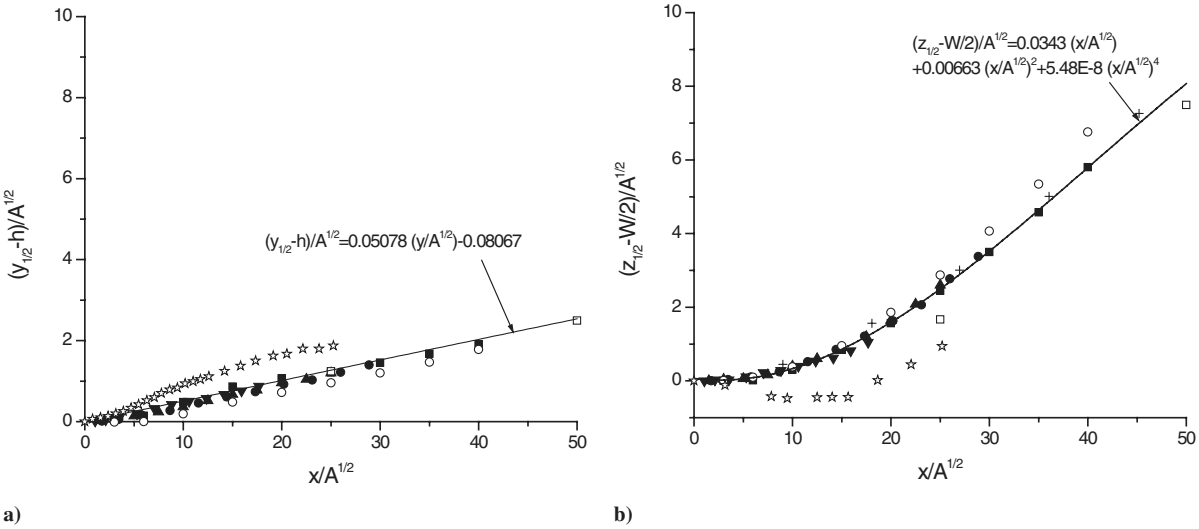

Fig. 9 Normalized streamwise development of the a) vertical half-widths and b) lateral half-widths of wall jets exiting the channel with $A_R = 1$ (■), $A_R = 3$ (●), $A_R = 4$ (▲), and $A_R = 8$ (▼), compared with previous results for wall jets exiting the long channel with $A_R = 1$ and $Re_h = 6 \times 10^4$ [22] (□), sharp-edged orifice with $A_R = 10$ and $Re_h = 3.4 \times 10^4$ [10] (★), wall jet exiting a round pipe with $Re_D = 1.1 \times 10^5$ [7] (○), and a wall jet exiting a round contoured nozzle with $Re_D = 1.7 \times 10^5$ [6] (+),

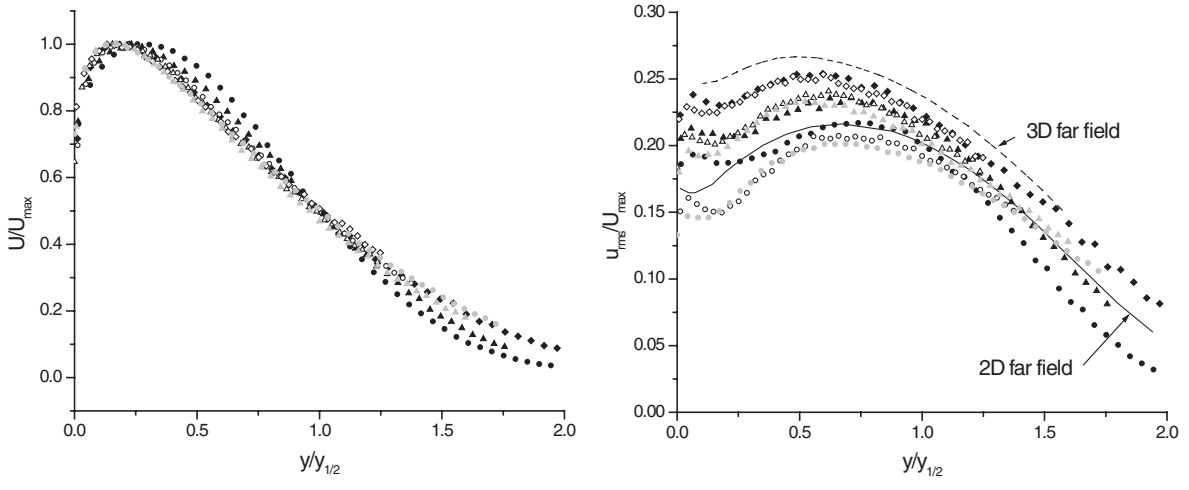

Fig. 10 Comparison of profiles of the a) mean velocity and b) turbulent velocity on the jet centerline at $x/\sqrt{A} = 15$ (○), $x/\sqrt{A} = 20$ (△), and $x/\sqrt{A} = 30$ (◇) for wall jets exiting the channel with $A_R = 1$ (filled symbols), $A_R = 4$ (open symbols), $A_R = 8$ (gray symbols), and the far field of a two-dimensional wall jet with $Re_h = 2 \times 10^4$ [23] (solid line), and a three-dimensional wall jet with $Re_D = 1.1 \times 10^5$ [5] (dashed line).

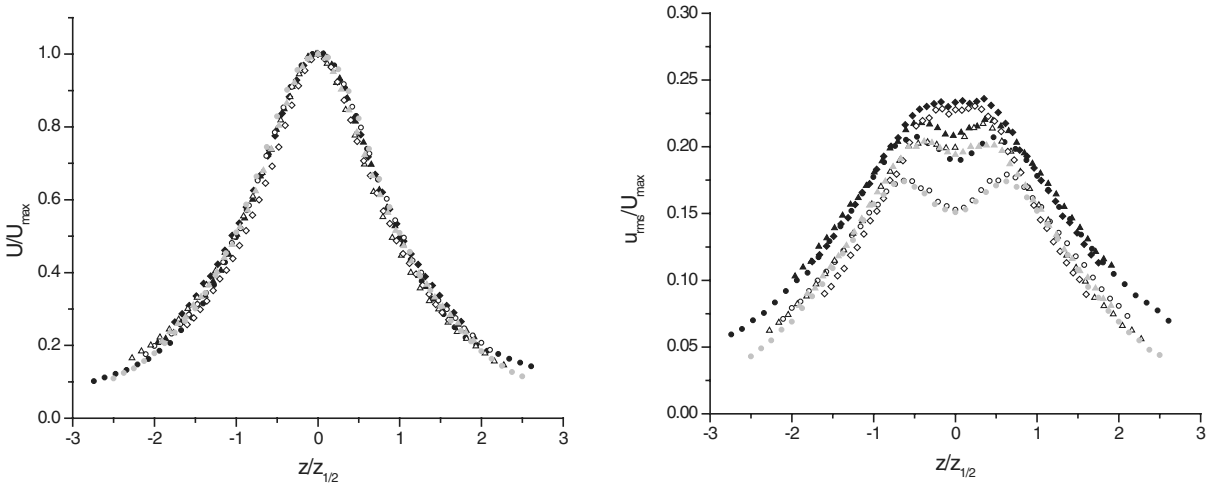

Fig. 11 Comparison of profiles of the a) mean velocity and b) turbulent velocity at $y = y_{max}$ for $x/\sqrt{A} = 15$ (○), $x/\sqrt{A} = 20$ (△), and $x/\sqrt{A} = 30$ (◇) for wall jets exiting the channel with $A_R = 1$ (filled symbols), $A_R = 4$ (open symbols), and $A_R = 8$ (gray symbols).

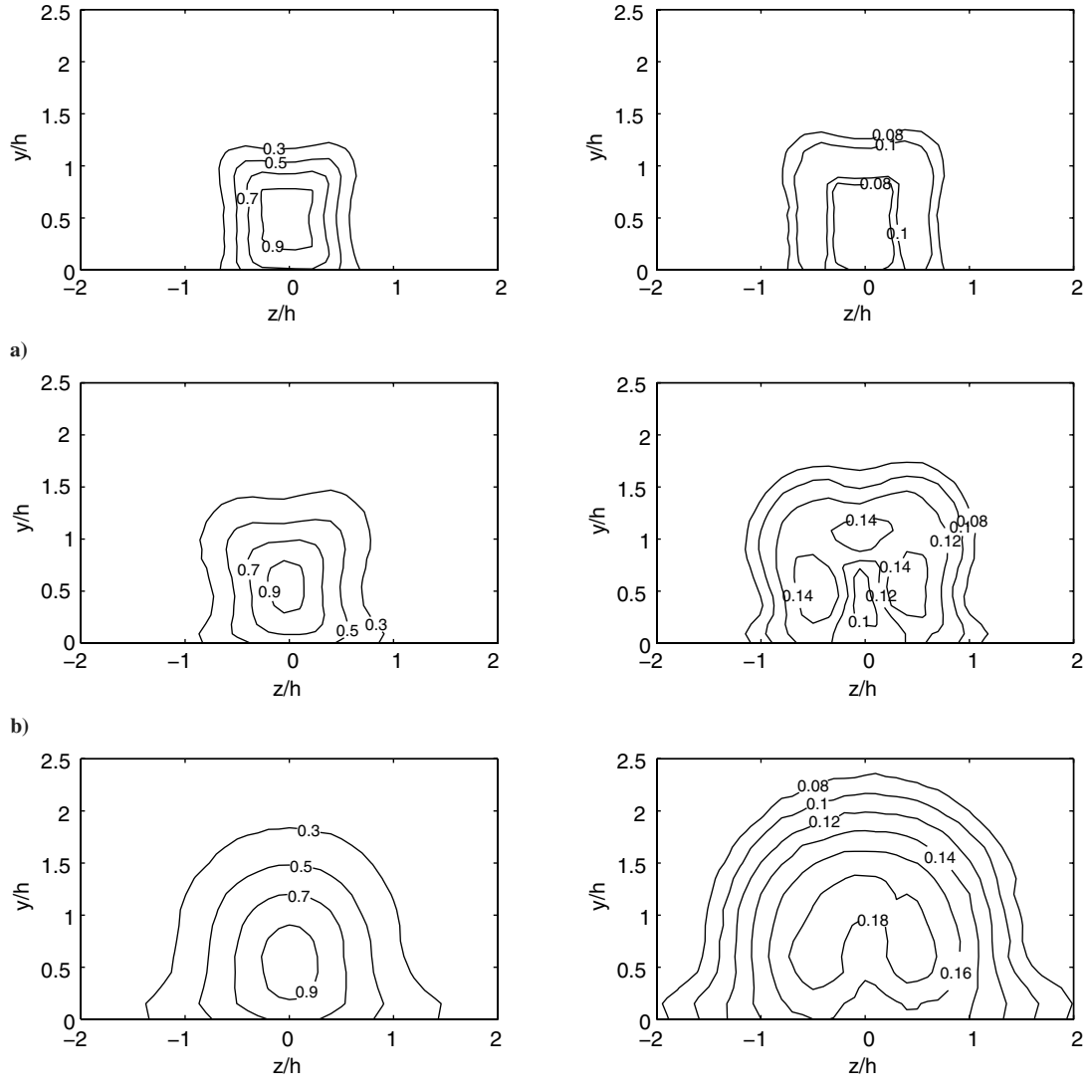

Fig. 12 Contours of the normalized mean streamwise velocity U/U_{max} (left) and the streamwise turbulence intensity u_{rms}/U_{max} (right) in the $A_r = 1$ wall jet at a) $x/h = 3$, b) $x/h = 6$, and c) $x/h = 10$.

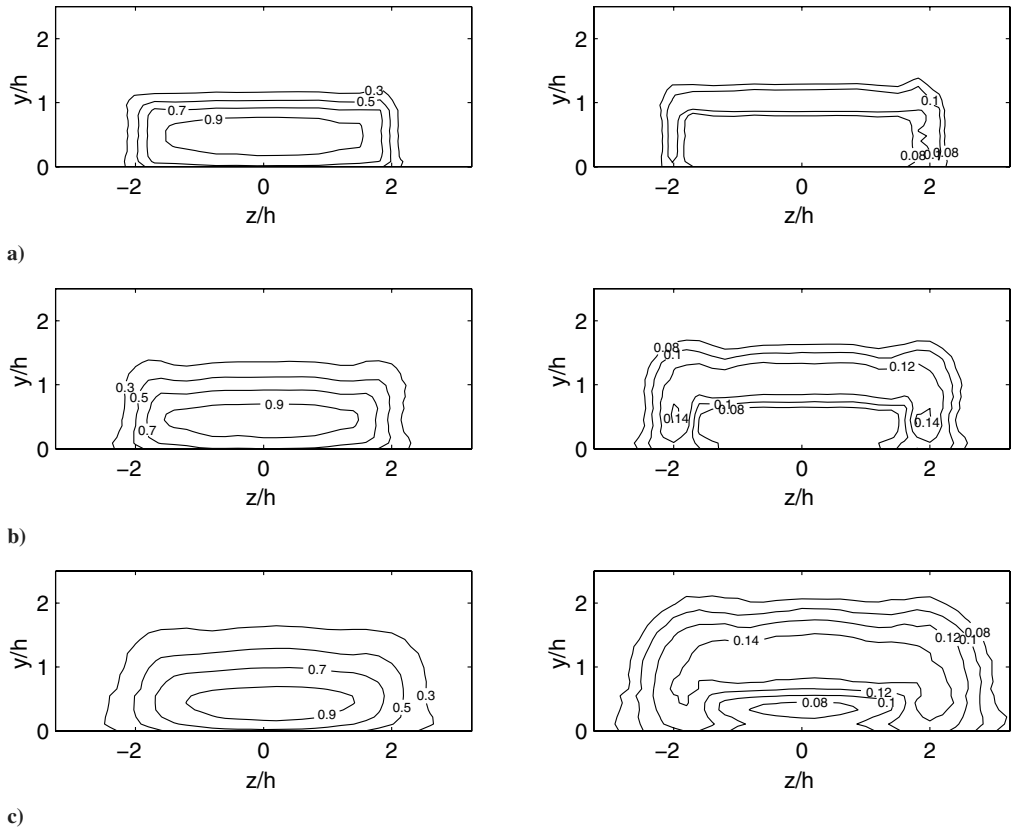

Fig. 13 Contours of the normalized mean streamwise velocity $U/U_{\max}$ (left) and the streamwise turbulence intensity $u_{\mathrm{rms}}/U_{\max}$ (right) in the $A_r = 4$ wall jet at a) $x/h = 3$, b) $x/h = 6$, and c) $x/h = 10$.

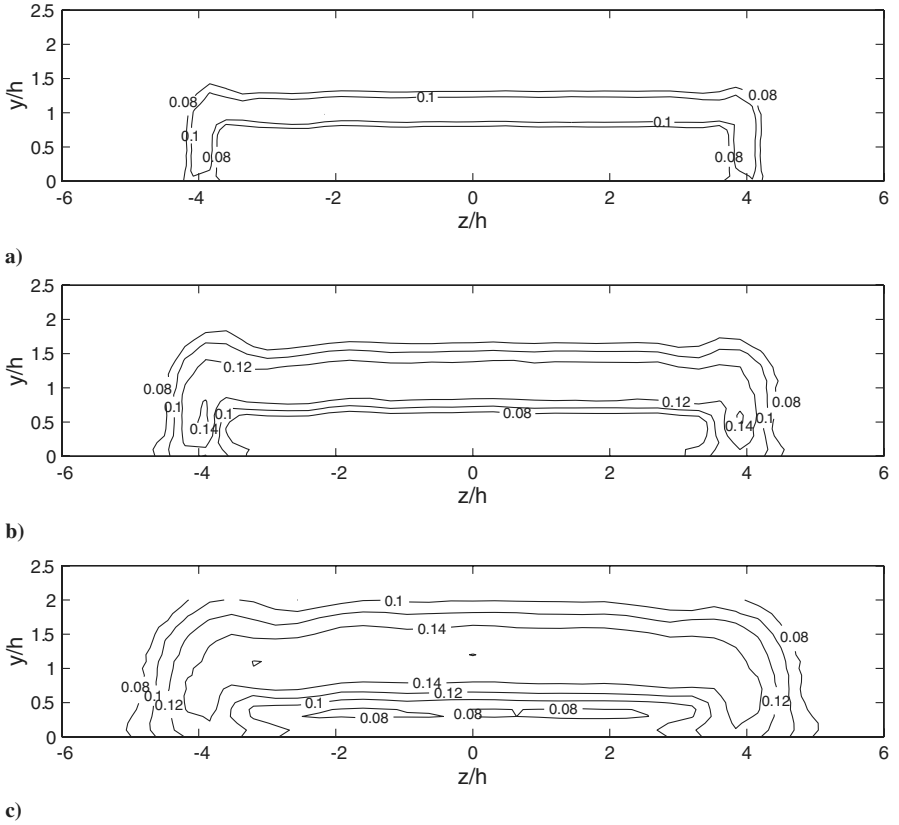

Fig. 14 Contours of the streamwise turbulence intensity $u_{\mathrm{rms}}/U_{\max}$ in the $A_r = 8$ wall jet at a) $x/h = 3$, b) $x/h = 6$, and c) $x/h = 10$.

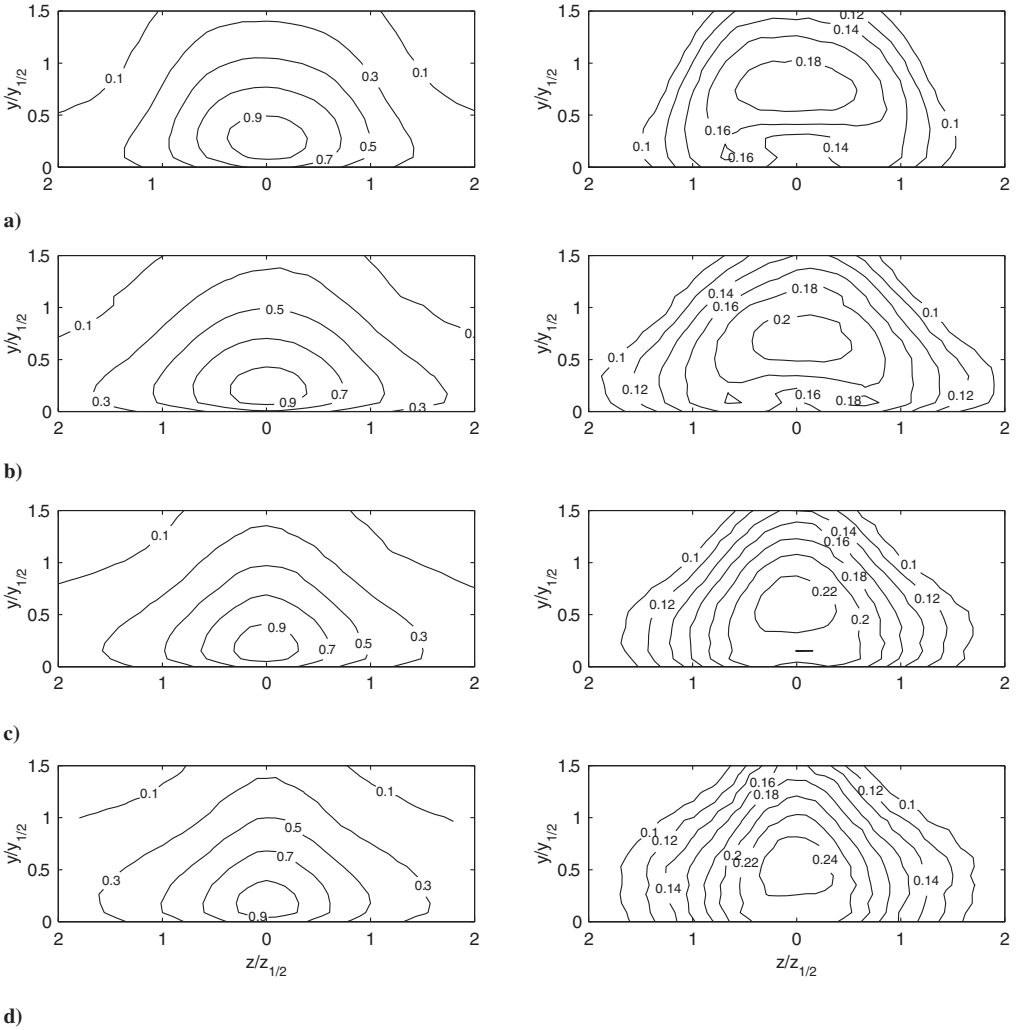

Fig. 15 Contours of the normalized mean streamwise velocity $U/U_{\max}$ (left) and turbulence intensity $u_{\rm rms}/U_{\max}$ (right) in the $A_r = 4$ wall jet at $x/\sqrt{A}$ equal to a) 10, b) 15, c) 20, and d) 30.

collapse reasonably well onto a single curve for the wall jets investigated here and for three-dimensional wall jets exiting round pipes [7] and round contoured nozzles [6]. The velocity decay in a three-dimensional wall jet exiting an $A_R = 10$ sharp-edged orifice [10] does not collapse nearly as well and is the only jet to clearly display the three proposed velocity decay regions when plotted in log–log fashion (shown using lines for this particular wall jet). The streamwise decay in the other wall jets is much more gradual than the orifice jet between $x/\sqrt{A} \approx 6$ to 20. In all cases, it appears that the radial decay region (far field) begins at roughly $x/\sqrt{A} \approx 20$.

The streamwise variation of the vertical and lateral half-widths with respect to the normalized streamwise coordinate $x/\sqrt{A}$ are shown in Fig. 9. To unify the data, the initial lateral half-width of the jet, $W/2$, or the initial vertical half-width, h, were subtracted from the related length-scales before normalizing by $\sqrt{A}$ to account for the differences in the initial size of the wall jets. The collapse of the present results onto a single curve is quite good. The lateral half-widths in a wall jet exiting an $A_R = 1$ channel considered previously [22] are slightly smaller than those reported here, but the growth of the half-widths are similar. The normalized length scales in a wall jet exiting a long round pipe [7] and a round contoured nozzle [6] are slightly larger than in the other jets because of differences in the initial three-dimensionality of these flows. A least-squares linear fit of the vertical half-widths measured here yields a vertical growth rate of 0.051, in reasonable agreement with the value of 0.059 reported by Fujisawa and Shirai [22] and with the generally accepted result of 0.048 ± 0.002 reported by Launder and Rodi [1]. The variation of the normalized lateral half-width was not linear in the region $x/\sqrt{A} \leq 40$, and so a fourth-order polynomial function was fit to the data, as shown in Fig. 9b.[‡] The lateral half-width determined from the fit was 5.5 times the vertical half-width at $x/\sqrt{A} = 40$, slightly higher than the values of 4.7 and 4.8 reported in the far field of a jet issuing from a round pipe [7] or a square channel [22], respectively. Again, the development of the three-dimensional wall jet using the $A_R = 10$ sharp-edged orifice is quite different from the other jets; in particular, the *vena contracta* caused by the orifice causes a decrease in the lateral half-widths and significantly larger vertical half-widths between $x/\sqrt{A} = 10$ and 30.

To better examine how the proposed scaling actually captures differences in the various wall jets, a comparison of the mean and turbulent velocity profiles normalized in terms of similarity variables at $x/\sqrt{A} = 15$, 20, and 30 for the $A_R = 1$ and 4 wall jets are shown in Figs. 10 and 11. Profiles at $x/\sqrt{A} = 14$ and 21 in the $A_R = 8$ jet and vertical profiles of the turbulent velocity from the far fields of two- and three-dimensional wall jets reported by Abrahamsson et al. [5,23] are also included for comparison. The mean velocity profiles at the centerline measured by Abrahamsson et al. are not included because there is little difference between the normalized velocity profiles in the far field of two- and three-dimensional wall jets. There were only small differences in the mean velocity profiles at each downstream location for a given wall jet and between the various wall jets. The turbulent velocity profiles, however, indicate that there are significant differences in the development of the different wall jets. For example, the peak in the turbulent fluctuations across the jet

[‡]As pointed out by one of the reviewers, this polynomial fit should only be used in the range $x/\sqrt{A} = 0$ to 40 and does not mean that the growth of the jet for $x/\sqrt{A} > 40$ continues to obey this function.

are significantly larger and closer to the jet centerline at $x/\sqrt{A} = 15$ in the $A_r = 1$ wall jet than in the larger-aspect-ratio jets at the same location. This indicates that the smaller-aspect-ratio jet is more fully developed than the larger-aspect-ratio jets. The differences in the profiles between the jets become smaller with increasing downstream distance. The peaks associated with the lateral shear layers eventually merge to form a single peak at $x/\sqrt{A} = 30$, signifying the end of the characteristic decay region and the onset of far-field three-dimensional wall-jet development.

The turbulent velocity profiles shown in Fig. 10b indicate that the central core region of the wall jet does, in fact, develop like a two-dimensional wall jet. For example, a comparison of the turbulent velocity profiles measured normal to the wall at $x/\sqrt{A} = 15$ with those measured by Abrahamsson et al. [5,23] indicates that the larger-aspect-ratio jets initially develop more like a two-dimensional wall jet in the far field than a three-dimensional wall jet. In terms of two-dimensional wall-jet scaling, the measurements in the two larger-aspect-ratio jets are at $x/h = 30$ and 40, respectively, distances that are consistent with the onset of far-field two-dimensional wall-jet development [23]. Further downstream, the lateral shear layers interact, causing the near wall peak in the turbulence profiles on the centerline to rapidly develop and exceed the values for the two-dimensional wall jet. By $x/\sqrt{A} = 30$, the profiles are similar to those measured in the far field of a three-dimensional wall jet, signifying the onset of far-field three-dimensional wall-jet development.

To better examine how the two-dimensional wall-jet core develops into a fully three-dimensional wall jet, velocity measurements were performed throughout the flowfield of each wall jet. Contours of the mean and fluctuating streamwise velocity in the near field of the $A_R = 1$ and 4 wall jets are shown in Figs. 12 and 13, respectively. In both wall jets, the mean flow initially resembles the channels they originated from, with the exception of a slight rounding of the mean flow contours at the corners. The lateral growth of both wall jets was initiated near the wall at the jet edges; obviously, this behavior could not be captured fully by the velocity profiles at the centerline or $y_{\max}$. In both jets, the turbulent fluctuations are initially the largest in the upper and lateral shear layers. As the $A_R = 1$ jet develops downstream to $x/h = 6$, three regions of large turbulent fluctuations associated with the upper and lateral shear layers are generated. The remains of a low-turbulence region that may be associated with the potential core of this jet is also apparent at the jet centerline, even though no evidence of it could be detected from the other measurements. Further downstream at $x/h = 10$, this region disappears and the three high-intensity turbulent regions merge to form a crescentlike region of strong turbulent fluctuations. The development of the turbulent flowfield in the $A_R = 4$ wall jet is quite different than for the $A_R = 1$ jet. The turbulence associated with the upper and lateral shear layers grows as the jet evolves downstream, however, the turbulent fluctuations grow the fastest on either side of the lateral shear layers near the wall. This suggests that the turbulent generated secondary flow that drives the lateral growth of the jet originates in the lateral shear layers. Similar behavior can also be observed in the turbulent flowfield for the $A_r = 8$ wall jet, shown in Fig. 14. The additional width of the channel separates the lateral shear layers even further, creating an even wider central region of two-dimensional wall-jet development off of the jet centerline.

The eventual collapse of the central region in the $A_R = 4$ wall jet can be observed in the mean and turbulent velocity fields, shown in

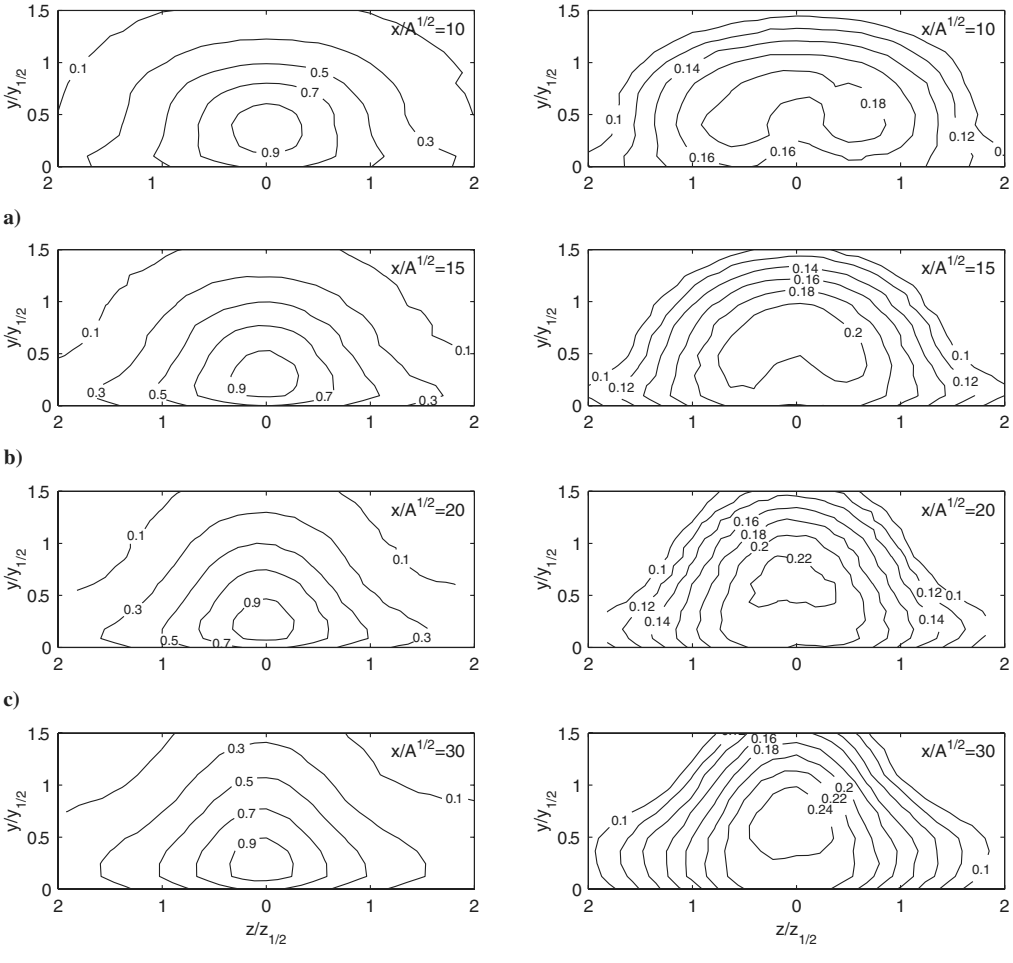

Fig. 16 Contours of the normalized mean streamwise velocity $U/U_{\max}$ (left) and turbulence intensity $u_{\rm rms}/U_{\max}$ (right) in the $A_r = 1$ wall jet at $x/\sqrt{A}$ equal to a) 10, b) 15, c) 20, and d) 30.

Fig. 15. The central region of lower turbulence intensity is apparent in the turbulent velocity contours at $x/\sqrt{A} = 10$ near the jet centerline. This region decreases in width due to the rapid growth of the lateral shear layers as the jet develops downstream, before eventually disappearing at $x/\sqrt{A} = 30$. Similar contours for the $A_R = 1$ wall jet are shown in Fig. 16. It is clear that this flow develops quite differently than the $A_R = 4$ wall jet. In particular, the contours of the maximum turbulence intensity at the core of the $A_R = 1$ jet display the characteristic crescent-shaped region until $x/\sqrt{A} = 30$. The contours of the mean and turbulent flowfield here begin to appear alike in the two jets, suggesting that this is approximately the onset of far-field jet development.

IV. Conclusions

The development of three-dimensional wall jets exiting rectangular channels with $A_R = 1$, 3, 4, and 8 was investigated in the region $x/h = 3$ to 60. The decay of the mean streamwise velocity and the development of the lateral and vertical jet half-widths normalized by the initial size of the channel in the different jets collapsed when the streamwise coordinate was scaled using the square root of the channel cross-sectional area. This method, though not as formally correct as using a virtual origin, has the benefit that no prior knowledge of the jet virtual origin is required. This method also has the additional benefit that it works well in the full range from the jet outlet to the onset of the far field. It is expected that this tool can be extrapolated to larger-aspect-ratio jets, however, no data are available for large-aspect-ratio wall jets, other than those formed using sharp-edged orifices, to verify this.

There were initially two regions of wall-jet development in the larger-aspect-ratio jets: a central, core region that evolves like a two-dimensional wall jet and an outer region associated with the lateral shear layers. Contours of the turbulent velocity field showed that the turbulent mechanism that causes the lateral spreading of the jet is initiated near the wall and on either side of the lateral shear layers. Increasing the aspect ratio of the channel separates the turbulent mechanism that causes the lateral growth of the jet, producing a wider region of two-dimensional wall-jet development and, in turn, a longer characteristic decay region that delays the onset of far-field three-dimensional wall-jet development. The profiles and contours indicate that the mean and turbulent statistics in the various wall jets begin to appear similar at $x\sqrt{A} = 30$, indicating that this is approximately the onset of far-field three-dimensional wall-jet development.

Acknowledgments

The authors gratefully acknowledge the financial support of the Natural Sciences and Engineering Research Council of Canada and the Ontario Graduate Scholarship program. The authors would also like to thank Peter Bender for his assistance in water jet cutting the channel used in this investigation.

References

[1] Launder, B. E., and Rodi, W., "The Turbulent Wall Jet," *Progress in Aerospace Sciences*, Vol. 19, Nos. 2–4, 1981, pp. 81–128.

[2] Launder, B. E., and Rodi, W., "The Turbulent Wall Jet-Measurements and Modelling," *Annual Review of Fluid Mechanics*, Vol. 15, 1983, pp. 429–459.

[3] Craft, T. J., and Launder, B. E., "On the Spreading Mechanism of the Three-Dimensional Turbulent Wall Jet," *Journal of Fluid Mechanics*, Vol. 435, 2001, pp. 305–326.

[4] Hall, J., and Ewing, D., "Investigation of the Large-Scale Structures in Large Aspect Ratio Three-Dimensional Wall Jets," Proceedings of the Fluids Engineering Division Summer Meeting, Houston, TX, American Society of Mechanical Engineers, Fluids Engineering Div., Paper 2005-77272, 2005.

[5] Abrahamsson, H., Johansson, B., and Lofdahl, L., "The Turbulence Field of a Fully Developed Three-Dimensional Wall Jet," Chalmers Univ. of Technology, Tech. Rep. 97-1, Sweden, 1997.

[6] Davis, M. R., and Winarto, H., "Jet Diffusion from a Circular Nozzle Above a Solid Plane," *Journal of Fluid Mechanics*, Vol. 101, 1980, pp. 193–218.

[7] Sun, H., and Ewing, D., "Effect of Initial and Boundary Conditions on the Development of Three-Dimensional Wall Jet," AIAA Paper 2002-0733, Jan. 2002.

[8] Law, A., and Herlina, "An Experimental Study on Turbulent Circular Wall Jets," *Journal of Hydraulic Engineering*, Vol. 128, No. 2, Feb. 2002, pp. 735–749.

[9] Rajaratnam, N., and Pani, B. S., "Three-Dimensional Turbulent Wall Jets," *Journal of the Hydraulics Division, American Society of Civil Engineers*, Vol. 100, No. HY1, 1974, pp. 69–83.

[10] Viets, H., and Sforza, P. M., "An Experimental Investigation of a Turbulent, Incompressible, Three-Dimensional Wall Jet," U.S. Air Force Office of Scientific Research, Technical Rept. 968, 1966.

[11] Sforza, P. M., and Herbst, G., "A Study of Three-Dimensional, Incompressible, Turbulent Wall Jets," *AIAA Journal*, Vol. 8, No. 2, 1970, pp. 276–283.

[12] Rajaratnam, N., *Turbulent Jets*, Elsevier, Amsterdam, 1976.

[13] Padmanabham, G., and Gowda, B., "Mean and Turbulence Characteristics of a Class of Three-Dimensional Wall Jets, Part 1: Mean Flow Characteristics," *Journal of Fluids Engineering*, Vol. 113, No. 4, 1991, pp. 620–628.

[14] Padmanabham, G., and Gowda, B., "Mean and Turbulence Characteristics of a Class of Three-Dimensional Wall Jets, Part 2: Turbulence Characteristics," *Journal of Fluids Engineering*, Vol. 113, No. 4, 1991, pp. 629–634.

[15] Trentacoste, N., and Sforza, P., "Further Experimental Results for Three-Dimensional Free Jets," *AIAA Journal*, Vol. 5, No. 5, 1967, pp. 885–891.

[16] Sfeir, A., "Investigation of Three-Dimensional Turbulent Rectangular Jets," *AIAA Journal*, Vol. 17, No. 10, 1979, pp. 1055–1060.

[17] Schwab, R. R., "Three-Dimensional Jets Formed Using Rectangular Orifices," Ph.D. Thesis, Queens Univ., Kingston, Ontario, Canada, 1988.

[18] Sun, H., "The Effect of Initial Conditions on the Development of the Three-Dimensional Wall Jet," Ph.D. Thesis, McMaster Univ., Hamilton, Ontario, Canada, 2002.

[19] Perry, A. E., *Hot-Wire Anemometry*, Clarendon Press, Oxford, England, U.K., 1982.

[20] Beuther, P. D., "Experimental Investigation of the Axisymmetric Turbulent Buoyant Plume," Ph.D., State Univ. of New York, Buffalo, New York, 1980.

[21] Hall, J. W., "The Role of The Large-Scale Structures in the Development of Turbulent Wall Jets," Ph.D. Thesis, McMaster Univ., Hamilton, Ontario, Canada, 2005.

[22] Fujisawa, N., and Shirai, H., "Mean Flow and Turbulence Characteristics of Three-Dimensional Wall Jet Along Plane Surface," *Transactions of the Japan Society for Aeronautical and Space Sciences*, Vol. 32, No. 95, 1989, pp. 35–46.

[23] Abrahamsson, H., Johansson, B., and Lofdahl, L., "A Turbulent Plane Two-Dimensional Wall-Jet in a Quiescent Surrounding," *European Journal of Mechanics, B/Fluids*, Vol. 13, No. 5, 1994, pp. 533–556.

N. Chokani
Associate Editor